NIF

DOE/NASA/51040-31
NASA TM-82646

High-Power Baseline and Motoring Test Results for the GPU-3 Stirling Engine

Lanny G. Thieme
National Aeronautics and Space Administration
Lewis Research Center

June 1981

Prepared for
U.S. DEPARTMENT OF ENERGY
Conservation and Renewable Energy
Office of Vehicle and Engine R&D

DOE/NASA/51040-31
NASA TM-82646

High-Power Baseline and Motoring Test Results for the GPU-3 Stirling Engine

Lanny G. Thieme
National Aeronautics and Space Administration
Lewis Research Center
Cleveland, Ohio 44135

June 1981

Work performed for
U.S. DEPARTMENT OF ENERGY
Conservation and Renewable Energy
Office of Vehicle and Engine R&D
Washington, D.C. 20545
Under Interagency Agreement DE-AI01-77CS51040

SUMMARY

In support of the Department of Energy's Stirling Engine Highway Vehicle Systems program, the NASA Lewis Research Center has installed a 7.5-kilowatt (10-hp) GPU-3 Stirling engine with a motoring dynamometer to continue to obtain data for validating Stirling-cycle computer simulations and to prepare for future component testing. The engine was originally built by General Motors Research Laboratories for the U.S. Army in 1965 as part of a 3-kilowatt engine-generator set.

Baseline tests were run to map the engine over a range of mean compression-space pressures of 2.8 to 6.9 megapascals (400 to 1000 psi) and engine speeds of 1500 to 3500 rpm with both helium and hydrogen as the working fluid. All tests were run at a heater-tube gas temperature of 677° C (1250° F). Maximum power obtained with hydrogen was 6.82 kilowatts (9.14 hp) at 6.9 megapascals (1000 psi) and 3500 rpm. The maximum power with helium was 4.26 kilowatts (5.71 hp) at 6.9 megapascals (1000 psi) and 2500 rpm. The highest brake thermal efficiencies obtained were 26.4 percent for hydrogen and 21.3 percent for helium. These both occurred at 6.9-megapascal (1000-psi) mean compression-space pressure and 1500-rpm engine speed.

The engine output was low at high speeds as compared with that for the previously reported low-power baseline tests that used the alternator and resistance load bank instead of the dynamometer. It is felt that this reduced power was caused by degradation of heat exchanger effectiveness as a result of contamination by rust and oil. However, efficiency was higher than in the previous tests because of the installation of a noncontaminated preheater that reduced combustion system losses.

Indicated power results were obtained as a function of mean compression-space pressure and engine speed for both helium and hydrogen. The maximum indicated power measured was 8.6 kilowatts (11.5 hp) for hydrogen.

Motoring tests were then run to aid in determining mechanical losses. Tests were completed over a range of mean compression-space pressures and engine speeds for both helium and hydrogen as the working fluid. The results were compared with the results of an energy-balance method for finding mechanical losses. The energy balance yields a linear variation of mechanical losses with engine speed, but the motoring results show a higher-order variation with speed. The two methods give results that are about the same at low speeds but differ significantly at high speeds.

INTRODUCTION

This work was done in support of the U.S. Department of Energy (DOE) Stirling Engine Highway Vehicle Systems program. The NASA Lewis Research Center, through interagency agreement DEAI01-77CS51040 with DOE, is responsible for management of the project under the program direction of the DOE Office of Vehicle and Engine R&D, Conservation and Renewable Energy.

As part of this effort Lewis is operating a 7.5-kilowatt (10-hp), single-cylinder, rhombic-drive Stirling engine. The engine was originally built by General Motors Research Laboratories for the U.S. Army in 1965 as part of a 3-kilowatt engine-generator set that was designated the GPU-3 (Ground Power Unit 3).

The GPU-3 Stirling engine test program at Lewis has three objectives:

(1) To obtain and publish detailed engine performance data
(2) To validate, document, and publish a NASA Lewis Stirling-cycle computer model
(3) To provide a test bed for evaluating new component concepts that evolve from supporting Stirling engine technology activities

After it was converted to a research configuration, the engine was tested with the original alternator and a resistance load bank to absorb the engine output. These test results are reported in reference 1. However, the alternator and load bank were not capable of absorbing the full engine output power. Thus following completion of these tests, the alternator was removed and the engine was installed with a motoring dynamometer. This allowed testing at the full engine output as well as running motoring tests to aid in determining mechanical losses.

This paper presents the results of both the high-power baseline tests and the motoring tests. Curves of engine output and brake specific fuel consumption as functions of engine speed and mean compression-space pressure are given for the high-power tests for both helium and hydrogen as the working fluid. These tests were run at a constant heater-tube gas temperature. Indicated power results are shown as determined by three methods: by an energy balance, by using pressure-volume diagrams, and by summing brake power and mechanical losses determined from motoring results.

For the motoring tests the cooler-regenerator cartridges were removed, and a special displacer was used to limit flow through the heat-exchanger circuit. The motoring power results are presented as a function of engine speed and mean compression-space pressure. Indicated gas work was also measured and used to correct the motoring power to arrive at an indication of the mechanical losses. Comparison is then made to energy-balance methods for determining the mechanical losses.

APPARATUS AND PROCEDURE - HIGH-POWER BASELINE TESTS

Engine Description and Background

The GPU-3 Stirling engine and dynamometer test bed are shown in figure 1. The engine as tested is a combination of parts taken from two identical GPU-3 units. The first of these was obtained from the U.S. Army Mobility Equipment Research and Development Center (MERDC) at Fort Belvoir, Virginia; the second was obtained through a loan from the Smithsonian Institution. These units were originally 3-kilowatt engine-generator sets built by General Motors Research Laboratories in 1965 for the U.S. Army. They were completely self-contained and capable of operating with a variety of fuels over a broad range of ambient conditions. The units were designed to use hydrogen as the working fluid. The GPU-3 engine is a single-cylinder, displacer engine with a rhombic drive and sliding rod seals. It is capable of producing a maximum engine output of approximately 7.5 kilowatts (10 hp) with hydrogen working fluid at 6.9 megapascals (1000 psi) mean compression-space pressure. The piston swept volume is 120 cubic centimeters (7.3 in^3).

The engine obtained from Fort Belvoir was initially torn down and restored to operating condition. It was then tested as part of the original GPU-3 with only those changes that were necessary to make the unit operable. Tests were run with both hydrogen and helium as the working fluid at various pressures

and at the design heater-tube gas temperature of 677° C (1250° F) and an engine speed of 3000 rpm. Comparisons were made with data taken by the Army in 1966. These results and a description of the original GPU-3 engine components and systems are given in reference 2.

The following changes were then made to convert the engine to a research configuration. The engine-driven accessories were removed (except for the oil system) with air, water, fuel, and working fluid supplied from the facility support systems. The original control system was replaced with manual controls. Where necessary, new parts were made, including new cooler-regenerator cartridges. Extensive instrumentation was added to obtain an energy balance, engine temperature profiles, conduction losses, working-space gas temperatures and dynamic pressures, and a measurement of indicated power. Finally, dimensional and volume measurements were completed as were steady-state flow tests on the various heat exchangers.

Baseline tests were run to map the engine over a range of heater-tube gas temperatures, mean compression-space pressures, and engine speeds with both helium and hydrogen as the working fluid. Tests were limited to the lower power levels (~4.5 kW (6 hp)) because the original alternator and a resistance load bank were used and they were not capable of absorbing the full engine output power. These results are presented in reference 1. The detailed data taken during those tests are included on microfiche as part of that report. Also given are the engine dimensions necessary for computer modeling as well as the results of the volume measurements and steady-state flow tests.

These data were used to make the initial direct comparisons with the Lewis computer simulation predictions. The simulation code is described in references 3 and 4. Results of the simulation comparisons with the test data are given in reference 4.

Test Setup

Following completion of the tests described in reference 1, the exhaust tubes of the preheater were flow-tested to check for blockage. About 45 percent of these tubes were plugged with soot from combustion; some leakage between tubes indicated that several of the tubes had holes burned through them. These findings explain the large circumferential temperature variation of the exhaust in these previous tests and also the low engine efficiencies that were measured. For the high-power tests it was decided to replace the preheater with the one from the Smithsonian engine. Flow tests on this preheater indicated only one tube blocked (of 560 tubes). This preheater was then instrumented and installed on the engine. Changes in instrumentation from that on the former preheater are given in appendix A.

Two separate crankcases were used during the high-power tests. The nylon timing gears failed under heavy load at the end of the helium baseline tests. This caused major damage to the crankcase of the Fort Belvoir engine, which had been used up to that time. For the hydrogen tests the crankcase from the Smithsonian engine was installed.

A schematic diagram of the GPU-3 test setup is shown in figure 2. Facility support systems shown include fuel, air, cooling water, oil, and working fluid. Also shown is the dynamometer for absorbing engine output. This schematic was updated from that given in reference 1. Numbers by the instrumentation symbols refer to instrumentation item numbers given in table III of reference 1. Only changes to the test setup from the previous tests are discussed here. A summary of changes to instrumentation in the support

systems is included in appendix A. For further details of the test setup see reference 1. The fuel, nozzle air, and combustion air systems were not changed.

A tank and pump were installed to supply the desired water flow rate to the engine's three cooling paths (buffer space, coolers, and nozzle). The water was not recirculated and its inlet temperature was not controlled. The inlet temperature was established by the temperature of the city water supplying the tank. The measurements of total water flow rate and temperature rise between outlet and inlet for the total flow were eliminated as it was found that the measurements in the individual water circuits were accurate and sufficient. To improve reliability, the thermopiles for measuring temperature rise in these individual circuits were replaced with ΔT probes with just one thermocouple per leg. The voltage signal representing the temperature rise was then amplified and recorded.

For the oil system the thermopile for measuring temperature rise was replaced with a ΔT probe (the same as the one described above for water).

Pressure transducers were added to the pressurization system to measure minimum cycle pressure in the compression and buffer spaces. The transducers were installed between check valves at the engine and needle valves in the pressurization lines, as shown in figure 2. These sections of line tend to trap their respective minimum pressures because of the one-way action of the check valves. Also, connections were made to the vent lines to allow taking working-fluid samples for later analysis.

The original GPU-3 alternator and resistance load bank were replaced by a universal dynamometer to absorb the engine output. This dynamometer is capable of 50 hp absorbing and 15 hp motoring and thus can absorb the full engine output. The alternator limited the previous tests to a maximum output of about 4.5 kilowatts (6 hp).

Two changes were made to improve the measurement of indicated power. Water-cooled adapters were installed for the expansion-space and compression-space miniature pressure transducers. These were added to minimize the transducers' zero shift and sensitivity change with temperature. Also, the shaft encoder was referenced to displacer top dead center (TDC = zero degrees shaft angle) by setting at the midstroke positions (90° before and after TDC) instead of at TDC. This method should be more accurate because of the much greater piston displacement per degree of crank travel at the 90° points than at TDC.

Finally, new modules were added to the recording system for the indicated work and dynamic pressure measurements. This updated system is shown in figure 3. The new modules are the indicated mean effective pressure (IMEP) modules for the compression, expansion, and buffer spaces; the two peak detector modules; and the two event detector modules. The IMEP modules are similar to that for the total IMEP measurement (compression-space pressure as a function of total working-space volume) described in reference 1. Each numerically integrates the associated pressure-volume diagram to obtain the work in terms of the IMEP. The value of IMEP calculated and displayed is an average value obtained over 100 engine cycles. The peak detector modules are used to find the maximum and minimum value of pressure for the miniature pressure transducers in the expansion, compression, and buffer spaces. The event modules determine the crank angle relative to displacer TDC at which the maximum and minimum values occur. The pressure signal that is input to these last four modules is determined by the selector switch shown in the middle of figure 3. References 5 and 6 provide more information on this type of instrumentation system.

The maximum and minimum values recorded from the peak detectors are shifted somewhat as a result of temperature effects on the transducers (although the water-cooled adapters minimized this effect). The true values for the compression and buffer pressures were found by using the pressure difference from the peak detectors along with the minimum values measured behind the check valves in the pressurization system. For the expansion pressure, only the difference between the maximum and minimum values could be determined.

The GPU-3 test setup is shown in figure 4. Recording systems and signal-conditioning equipment are shown on the left, with the engine and dynamometer on the right. Steady-state data were recorded and printed out on a data logger. Dynamic data were taken with both an oscillograph recorder and an oscilloscope.

Test Procedure

The desired test matrix range for both the helium and hydrogen runs included mean compression-space pressures of 2.8 to 6.9 megapascals (400 to 1000 psi) and engine speeds of 1500 to 3500 rpm. The heater-tube gas temperature and cooling-water inlet temperature were not varied for these tests. The heater-tube gas temperature was measured with thermocouple probes installed inside three of the 40 heater tubes and spaced circumferentially around the heater head. The maximum reading of these three thermocouples was manually controlled to 677° C (1250° F) by adjusting the fuel flow with a needle valve. The cooling-water inlet temperature was not controlled and varied from 19° to 21° C (66° to 70° F) over the series of tests.

On each engine startup, cooling-water flow was first provided to the engine and the mean compression-space pressure was set at approximately 2.1 megapascals (300 psi). Combustion was then started with no. 1 diesel fuel (lower heating value, 18 590 Btu/lb) from the startup fuel tank. As the heater-tube gas temperature approached 540° C (1000° F) the engine was started rotating by motoring with the dynamometer. Engine warmup conditions were then set to 2.8-megapascal (400-psi) mean compression-space pressure, 677° C (1250° F) heater-tube gas temperature, and 2000-rpm engine speed. When the engine temperatures were sufficient to sustain operation, the dynamometer motor was shut off. The engine was stabilized at the reference condition listed above to allow it to reach operating temperatures. About 30 minutes of warmup time was necessary.

Generally, one curve at constant mean compression-space pressure, heater-tube gas temperature, and cooling-water flow was run after each engine start-up. The curve consisted of data points taken at engine speeds varying by 500-rpm intervals, with the highest speed set first. At each point the speed was set by adjusting the speed control on the dynamometer. The combustion airflow was set to maintain an air-fuel ratio of about 35 to 1. After the desired conditions were reached, the fuel run tank was valved to the engine. These conditions were then maintained for 15 minutes. All steady-state data were recorded three times and dynamic data once during this period. The startup fuel tank was then again valved to the engine, and the next data point established. The fuel flow was determined from the initial and final weights of the fuel run tank. This procedure was repeated for each data point.

RESULTS AND DISCUSSION - HIGH-POWER BASELINE TESTS

The results of the high-power baseline tests are presented in figures 5 to [illegible]. These figures are summarized as follows:

The influence of mean compression-space pressure and engine speed on engine output and brake specific fuel consumption (bsfc) is shown in figures 5 and 6. The engine data obtained with the dynamometer are compared with previous engine data obtained with the alternator in figure 7. The differences indicated by this comparison are explained with the aid of figures 8 to 12. Figures 13 and 14 give examples of energy balances obtained on the engine. Finally, indicated power results as a function of mean compression-space pressure and engine speed are shown in figures 15 and 16. The detailed data taken during these tests are not included as part of this report but are available from the author. A sample data point to indicate what is available is given in appendix A.

Engine Performance with Helium and Hydrogen

Figure 5 illustrates the effect of engine speed and mean compression-space pressure on engine performance with helium working fluid. The same is shown in figure 6 for hydrogen working fluid. The heater-tube gas temperature was 677° C (1250° F), and the average cooling-water inlet temperature was 20° C (68° F) for both series of tests. Of the three steady-state data scans taken at each operating condition, two were reduced and plotted. When both scans gave approximately the same results, only one symbol was plotted for that condition.

An extra point at an engine speed of 1000 rpm and a mean compression-space pressure of 2.8 megapascals (400 psi) with helium working fluid was added to the planned test matrix. Also, several points at the low pressures and high engine speeds could not be run. This was due to the engine output being inadequate at those conditions for the engine-dynamometer system to sustain operation.

The maximum engine output with helium working fluid was 4.26 kilowatts (5.71 hp) at a mean compression-space pressure of 6.9 megapascals (1000 psi) and an engine speed of 2500 rpm. The lowest bsfc was 390 g/kW-hr (0.64 lb/hp-hr) at 6.9 megapascals (1000 psi) and 1500 rpm. This corresponds to a brake thermal efficiency of 21.3 percent.

With hydrogen working fluid the maximum power obtained was 6.82 kilowatts (9.14 hp) at 6.9 megapascals (1000 psi) and 3500 rpm. The minimum bsfc was 315 g/kW-hr (0.52 lb/hp-hr) at 6.9 megapascals (1000 psi) and 1500 rpm. This corresponds to a brake thermal efficiency of 26.4 percent. This efficiency is in the same range as that obtained by General Motors (ref. 7).

In addition to the fact that both the engine output and efficiency are greater with hydrogen working fluid than with helium, the figures show that the engine output tends to peak at a higher speed with hydrogen. The increase in bsfc is also much less at the higher speeds with hydrogen than with helium. These results are indications of the lower flow losses through the heat exchangers when using hydrogen as the working fluid. This effect has been substantiated by computer simulation predictions.

Comparison of Engine Output with Previous Data Obtained with the Alternator

Figure 7 shows a comparison of the engine output with data obtained previously in the low-power baseline tests that used the original GPU-3 alternator and a resistance load bank to absorb the output. Reference 1 describes the low-power baseline tests in detail. The hot- and cold-end temperatures were not identical for these two series of tests. For the high-power dynamometer tests the heater-tube gas temperature was 677° C (1250° F) and the cooling-

water inlet temperature was 20° C (68° F). For the low-power alternator tests the heater-tube gas temperature was 650° C (1200° F) and the cooling-water inlet temperature was in the range 13° to 15° C (56° to 59° F). However, as both temperatures were higher for the dynamometer tests, the effects of the two should somewhat offset each other.

With the exception of one point at 4.1 megapascals (600 psi) hydrogen data from the low-power alternator tests were limited by the allowable alternator current to curves for 1.4 and 2.8 megapascals (200 and 400 psi). As data were taken for pressures of 2.8 megapascals (400 psi) and higher for the high-power dynamometer tests, comparison could only be made at 2.8 megapascals (400 psi) for hydrogen as the working fluid. Also, some of the previous helium tests were limited by the alternator to high speeds, particularly for high pressures; therefore comparisons again are incomplete.

The engine power outputs from the two series of tests were about the same for the lower part of the speed range (with the exception of the 2.8-megapascal (400-psi) curves for helium). However, there are large discrepancies at the higher speeds. Thus the variation in output appears to be related primarily to speed.

Increasing pressure drop through the heat exchangers could cause this type of effect. Figure 8 shows the set of eight cooler-regenerator cartridges as well as three of the end caps that connect the coolers to the compression space. In areas where the working fluid is present - around the regenerator can, at the outlet of cooler tubes, and around the end cap - there were significant deposits of what was analyzed to be a combination of oil and rust. Rust occurs during teardowns when the engine parts are exposed to the atmosphere. Also, rusting may take place when the assembled engine is left unpressurized as a result of severe engine leaks. The engine was cleaned before each reassembly, but obviously some of the rust was not removed. The oil contamination was from oil pumped past the sliding shaft seals during engine operation.

Steady-state flow tests were run on the various heat exchangers to measure the pressure drop. Air at 793-kilopascal (115-psi) inlet pressure was used for the calibration, with pressure drop as a function of mass flow rate being recorded. Mass flow rates were chosen to give about the same range of Reynolds number as actually occurs in the engine. This range was predicted by the Stirling simulation computer program. For further explanation of steady-state flow tests on the heat exchangers, see reference 1.

Figure 9 shows pressure drop as a function of flow rate for the heater head assembly after the high-power tests with the dynamometer and after the low-power tests with the alternator. This includes flow through all the heat exchangers - coolers, regenerators, and heater. The mass flow rates through the heater head assembly are eight times the flow rates shown in the next two figures for the individual cooler-regenerator cartridges. This is due to the eight cooler-regenerator paths in the heater head. The test for the heater head assembly was made for flow in both directions. The pressure drop has increased by about 10 percent over most of the flow range for the latest flow tests.

Throughout the GPU testing three of the cooler-regenerator cartridges were flow tested at various intervals. Figure 10 gives flow test results for these three when they were new, after 80 hours of engine testing (after the low-power tests with the alternator), and after 191 hours of engine testing (after the high-power tests with the dynamometer).

The pressure drops through the cartridges have been increasing throughout the testing except for one of the cartridges between 80 and 191 hours. Also,

the spread from the least pressure drop to the greatest pressure drop has increased by a large amount.

The range of pressure drops for all eight cooler-regenerators following the high-power test with the dynamometer is shown in figure 11. At the maximum flow rate tested, 18 g/sec (0.04 lb/sec), the pressure drop ranged from about 234 to 421 kilopascals (34 to 61 psi). This compares with a range of 165 to 196 kilopascals (24 to 28.5 psi) when the cartridges were new. The large spread for the cartridges after 191 hours of testing indicates that there was poor distribution of flow through the eight cooler-regenerator circuits during these engine tests.

The difference in pressure drop through the heater head assembly shown in figure 9 does not appear to be large enough to solely account for the differences in engine output at high speeds. This is substantiated by the NASA Lewis Stirling cycle computer program. However, what effect the contamination of the heater head had on heat transfer in the heat exchangers is not known. Figure 8 shows deposits on the water side of the cooler tubes, so this would also have adversely affected the heat transfer. Estimates of new heat transfer coefficients for the heat exchangers would have to be made to further analyze the differences.

Two other areas whose effects were included in figures 5 and 6 were investigated in attempting to determine the reasons for the decrease in engine output. The first concerned the accuracy of the torque measurement. To check this, a torquemeter and a 7.5-kilowatt (10-hp) electric motor were used to calibrate the dynamometer system. The torquemeter was calibrated and then installed between the electric motor and the dynamometer (after the engine was removed from the test stand). Tests were run over a range of loads for each speed with the load cell torque reading for the dynamometer system being compared with that from the torquemeter. After analyzing the results, it was decided to add a constant value of 0.6 lb-ft to each value of torque as measured by the load cell.

The second area investigated related to check valve losses. Prior to the start of the high-power tests with the dynamometer, new check valves were installed in the vent lines of the buffer and compression spaces. These two lines are tied together and vented through a single needle valve. A pressure transducer was installed in the common line to determine if these check valves were working properly. Typical pressure traces obtained are shown in figure 12 for three speeds. Large oscillations are shown at the higher speeds, with little or none at the lower. These oscillations indicated that the check valves were opening at the higher speeds and thus allowing direct communication between the buffer and compression spaces. An attempt was made to determine this effect on the engine output at 3000 rpm by installing a needle valve in the line between the two check valves. A data point was taken with the valve open and closed, but no difference in engine output was detected. Consequently, the tests were concluded with these check valves in place.

However, motoring tests were run following the high-power baseline tests. These motoring tests, with fewer operating constraints and control restrictions to mask the results, gave the capability for determining the magnitude of the losses that were not detected during the engine tests. The motoring tests are described elsewhere in this report. Tests were run at various speeds and pressures with hydrogen and helium and with the needle valve in the vent line open and then closed. The losses were primarily a function of speed. It was decided to use the following correction factors:

Speed, rpm	Correction, kW (hp)
1500, 2000	0 (0)
2500, 3000	.10 (0.13)
3500	.34 (0.46)

These values were added to the measured engine power outputs. Note that the correction is only significant at 3500 rpm.

Thus the results given in figures 5 and 6 have been corrected for both factors: the torque measurement correction and the correction due to losses associated with the check valves. The latter correction was applicable to only the three highest pressure curves for hydrogen and for the 4.1-megapascal (600-psi), 3000-rpm point for helium. All other data were run with the needle valve in the vent lines closed to minimize the losses.

Energy-Balance Results

Energy balances obtained on the engine during these tests and during the low-power tests with the alternator are compared in figure 13 with hydrogen as the working fluid. A common point of 2.8-megapascal (400-psi) mean compression-space pressure and 1500-rpm engine speed is used. The hot- and cold-end temperatures are somewhat different, but the effects of these differences should tend to offset each other.

Although the engine output is about the same for each, the efficiency increased from 14.9 percent for the alternator test to 19.3 percent for these dynamometer tests. The main reason for this efficiency increase was the lower exhaust losses. The exhaust losses were substantially decreased by changing preheaters and by lowering the air-fuel ratio. The air-fuel ratio was decreased from 49 for this particular point of the alternator tests to about 35 for the dynamometer tests. Also, as described in the Test Setup section the former preheater had almost one-half of the exhaust tubes plugged and holes burned through some of the tubes. It was replaced with the preheater of the engine obtained from the Smithsonian Institution.

The heat losses to the oil and buffer water; the cycle heat rejection (defined as the heat loss to the water passing through the coolers minus the conduction losses); and the conduction, radiation and convection, and nozzle water losses are essentially the same for both cases. However, they have increased as a percentage of the heat input for the dynamometer tests because of the lower heat input resulting from the lower exhaust losses.

The efficiency gain was obtained at most of the data points that could be compared with the previous low-power alternator test results. Thus the increase in combustion system efficiency (lower exhaust losses) more than offset the decrease in thermodynamic cycle efficiency (contaminated regenerators and coolers).

Figure 14 compares energy balances for helium and hydrogen working fluids at 6.9-megapascal (1000-psi) pressure and 1500-rpm engine speed. This was the maximum efficiency point for each working fluid during the dynamometer tests.

Note that the maximum efficiency was 21.3 percent for helium and 26.4 percent for hydrogen. Differences in efficiency and engine output between the two working fluids are not as significant at the lower speeds as at the higher speeds. At the maximum speed of 3500 rpm for 6.9-megapascal (1000-psi) pressure the respective efficiencies were 8.6 percent for helium and 19.8 percent

for hydrogen. Again, this larger difference is primarily due to the higher flow losses with helium.

The power in from the fuel was approximately the same for each point shown: 15.8 kilowatts (21.1 hp) for hydrogen and 15.4 kilowatts (20.7 hp) for helium. Also, the exhaust losses as well as the conduction, radiation and convection, and nozzle water losses were about the same; therefore the heat into the working fluid was approximately equal for each point. The energy balances indicate then that the increase in efficiency with hydrogen comes from an increase in engine output due to decreasing cycle heat rejection and heat losses to the oil and buffer water. The heat loss to the oil and buffer water can be taken as an indication of the engine mechanical losses. The mechanical losses are lower with hydrogen working fluid than with helium because of the lower gas work losses in the buffer space for hydrogen.

Indicated Power Results

Figures 15 and 16 give indicated power results as computed by several methods. The measurement of indicated power is useful for direct comparison with engine output as determined by most computer simulations and also for isolating the Stirling-cycle effects on engine output.

Figure 15 shows indicated power as a function of engine speed and mean compression-space pressure for both helium and hydrogen working fluids. It compares indicated power obtained from energy balances with that obtained from pressure-volume (p-v) diagrams. The hot- and cold-end temperatures were the same as shown in figures 5 and 6.

The energy-balance results assume that the heat losses to the oil and buffer water represent the engine mechanical losses. These are then added to the engine brake output to get the indicated power. The p-v diagram results were obtained from separate p-v diagrams for the expansion and compression spaces. The power from the compression-space diagram is subtracted from that of the expansion-space diagram to get the indicated power. The instrumentation system to obtain these p-v diagrams is described in reference 1 and in the Test Setup section of this report.

The two methods compare well for hydrogen working fluid. The p-v results are lower at low speeds and higher at high speeds than in the energy-balance results. This trend was generally true for the results for both hydrogen and helium from the tests reported in reference 1. Only several preliminary p-v diagrams were shown in that reference because of inadequacies in the p-v measurement system; this was mainly due to the lack of water cooling on the pressure transducers, which could have resulted in a sensitivity shift with temperature. Thus although approximately the same trend was obtained, the results were less consistent in the earlier tests.

For helium the p-v diagrams gave results that were higher at all points than were those for the energy-balance method. As this trend is not consistent with previous data (even with helium) and as the energy-balance results agree with expected values, these helium p-v results appear to be questionable.

Considering all p-v results from both alternator and dynamometer testing, the hydrogen data are more consistent in their trends and comparisons than are the helium data. This may indicate a response problem with the helium pressure measurements although calculations show that the response times should be adequate. The main concern is in the expansion-space pressure measurement where the transducer is located at the end of a 15.2-centimeter (6-in)-long tube. The compression-space transducer is approximately flush-mounted.

The maximum indicated power for hydrogen is 8.6 kilowatts (11.5 hp) at 6.9-megapascal (1000-psi) mean compression-space pressure and 3500-rpm engine speed. Indicated power results for 6.9-megapascal (1000-psi) helium appeared to be in error and are not reported. The indicated power curves tend to peak out at slightly higher speeds than do the brake power curves. This is expected as the mechanical losses increase with speed.

Figure 16 compares p-v indicated power results for hydrogen both from two p-v diagrams and from one p-v diagram. The use of two diagrams is as stated previously (expansion-space work minus compression-space work), and these results are the same as those shown in figure 15. The indicated power can also be approximated with one diagram by using any pressure in the working space (compression-space pressure is used in these tests) versus the total change in working-space volume.

The results indicate that the use of one diagram gives a somewhat higher answer than does the use of two diagrams. This has been consistent for most testing and particularly with hydrogen. There are problems associated with either method. The two-diagram method involves finding a small answer by taking the difference between two large numbers, each of which has measurement errors involved. The one-diagram method neglects the full effect of pressure drop through the heat exchangers as only one pressure is used. On the basis of all data taken to this time, the use of separate p-v diagrams in the expansion and compression spaces appears to give the more accurate results.

APPARATUS AND PROCEDURE - MOTORING TESTS

Test Setup

Motoring tests were run to aid in determining engine mechanical losses, which can be added to the brake power to get the engine indicated power. Several other methods, in addition to motoring, are also used to determine the mechanical losses and indicated power; thus each can be compared with the others to evaluate the results. The other methods use energy-balance data to determine mechanical losses (heat to the oil and buffer-space cooling water) and direct measurement of the indicated power with pressure-volume diagrams.

Motoring a Stirling engine to determine its mechanical losses cannot be effectively accomplished by driving the engine in its normal configuration. To properly motor, the displacer piston must be replaced with a piston of the same weight but causing negligible pumping. For these tests a solid displacer piston was made with six holes drilled through the piston to allow direct flow between the compression and expansion spaces and to eliminate flow through the heat exchangers. The weight was made identical to that of the normal hollow stainless-steel displacer by fabricating this piston from a combination of aluminum and magnesium. As the motoring tests were run cold (no combustion occurring), these materials did not need to be heat resistant. The holes drilled through the displacer had a diameter of 0.95 centimeter (0.375 in.) and were sized to give a flow area about 1.5 times the heater-tube flow area. The piston rings were installed in the same manner as for the standard displacer. The displacer piston for motoring is shown in figure 17.

A further problem with motoring is the different loads on the bearings, seals, and piston rings as compared with engine operation because of the difference in pressure variations. This effect was reduced by changing the volume of the working space to give approximately the same pressure ratio during motoring as occurs in normal engine operation. The eight cooler-regenerator cartridges were removed and replaced with plugs to eliminate a substantial

amount of volume. As the temperature effec' on pressure ratio are minimal during motoring, an estimated pressure ratio could be calculated from the known volumes. The actual pressure ratios were measured during the motoring tests. Those results are given in the Results and Discussion section. One of the plugs that replaced a cooler-regenerator cartridge is also shown in figure 17. As no combustion was necessary for these tests, the preheater was removed from the engine.

The facility setup was the same as in figure 2 with the following changes. The air and fuel systems and the nozzle water lines were disconnected. The turbine flowmeter in the cooler water line was replaced with a flowmeter of less range as the flow was reduced because of the plugs in the cooler passages. A small water flow was circulated around the plugs and around the cylinder cooling passage to reduce the temperature variations of the working fluid during motoring.

A second set of nylon timing gears failed at the end of the hydrogen baseline tests. For the motoring tests these were replaced with a set of aluminum timing gears. Also, a coupling with greater torsional flexibility was installed between the engine and dynamometer to aid in reducing the effect of torque reversal on the timing gears.

Test Procedure

The motoring test matrix for both helium and hydrogen working fluids consisted of mean compression-space pressures from 1.4 to 6.9 megapascals (200 to 1000 psi) and engine speeds from 1500 to 3500 rpm.

On each startup, cooling-water flow was first provided to the buffer and cooler circuits. Cooling-water inlet temperature was not controlled and varied from 4° to 8° C (40° to 47° F) for these tests. Approximately 2.8-megapascal (400-psi) mean compression-space pressure was set in the engine, and the engine was then rotated by motoring with the dynamometer. Motoring conditions were maintained at 2.8-megapascal (400-psi) pressure and 2000-rpm engine speed until the oil temperature reached 38° to 41° C (100° to 105° F). This took about 30 minutes. Oil temperature was not controlled during these tests; variations in oil temperature were similar to those in normal engine operation.

Following engine warmup, one or two curves at constant mean compression-space pressure were run for each engine startup. A curve consisted of data points taken at engine speeds varying by 500-rpm intervals, with the highest speed set first. The speed was set by adjusting the speed control on the dynamometer. After the desired conditions were established, the data point was held for about 10 minutes. During this time steady-state data was recorded three times and dynamic data once. After completing this, a new speed was set and the procedure repeated.

RESULTS AND DISCUSSION - MOTORING TESTS

The figures presenting the motoring results are summarized as follows: The measured motoring power is given in figure 18 as a function of speed and pressure. Figure 19 compares mechanical losses (as found by energy balances) for both the motoring tests and the engine tests to verify that both results are about the same. Figures 20 and 21 illustrate the correction of the motoring power by subtracting the indicated work of the working fluid. The mechanical losses as determined by this correction are then compared with energy-balance results in figures 22 and 23.

The plotted points in figures 18 to 23 are averages of all data taken for a particular condition. Each curve with helium working fluid was run twice. For hydrogen working fluid, only the 6.9-megapascal (1000-psi) curve was repeated before the displacer piston failed and the motoring tests were ended. Some difficulty was found in obtaining repeatable data. As the reason for this was not determined, it was decided to average all acceptable data for a given point. The average difference between the results for running a data point several times was about 10 percent.

Determination of Mechanical Losses from Motoring Results

Figure 18 shows the motoring power as a function of mean compression-space pressure and engine speed for helium and hydrogen working fluids. The motoring power is the power needed to drive the engine with the dynamometer motor at the desired engine speed and mean compression-space pressure. The motoring power was determined from the dynamometer load cell reading. The slopes of the curves are increasing with engine speed, indicating a more than linear variation with speed. Also, note the large values of motoring power that were measured. At maximum pressure and speed the motoring power was 3.5 kilowatts (4.7 hp) for hydrogen working fluid and 4.5 kilowatts (6.0 hp) for helium. This difference also shows that a greater motoring power was required with helium working fluid than with hydrogen at any given condition.

A comparison was made with engine test data to determine if the mechanical losses for motoring were approximately the same as during engine testing. This was done on the basis of mechanical losses as measured from the energy balance (heat to oil plus heat to buffer-space cooling water). Figure 19 shows this comparison for two pressure levels for both helium and hydrogen working fluids. The curves for engine test results are an average for runs from testing with the alternator and with the dynamometer. The figure indicates that the results are about the same, with the motoring values being somewhat less than the engine values for higher pressures. This may be due to less heat conduction to the buffer-space cooling water during motoring tests as the cold-end metal temperatures were lower for the motoring tests than for engine tests.

Measurements of the indicated work of the working fluid were made during the motoring tests through the use of pressure-volume diagrams. The work was determined by two methods. The first was to use separate p-v diagrams in the expansion and compresson spaces with the total work being the difference between expansion work and compression work. This gave negative values of work, as is expected as work is being done on the gas. The other method was to use just one p-v diagram, that being the compression-space pressure as a function of the total volume change of the working space. This also gave negative values as expected.

The work determined from the one p-v diagram was more consistent than that found from two diagrams. It is probable that the error involved in subtracting two large numbers (as in expansion work minus compression work), each of which has a certain error, becomes excessive when determining the small values of gas work involved in motoring. The one-diagram method does not properly account for pressure drop losses in the working space, and these errors appear to be important for engine testing. However, for motoring the pressure drop losses are small as a result of removing the cooler-regenerators and using the displacer with holes. Thus it was decided for the motoring tests that the indicated gas work is best determined from one p-v diagram.

Figure 20 gives indicated work results measured by the one-diagram method. These results are plotted as a function of mean compression-space

pressure and engine speed for both helium and hydrogen working fluids. Note that the values for helium are significantly higher than those for hydrogen. These indicated work results represent losses in the working fluid due to flow losses, irreversibilities, and leakage between the compression and buffer spaces; these losses should not be charged against the mechanical losses for the engine. Thus a first-order attempt to separate these can be made by subtracting the working-fluid indicated power from the total motoring power.

Buffer-space gas work was also measured, but any losses occurring in the buffer space, including gas work, are lumped in with the mechanical losses.

Figure 21 shows the mechanical losses as determined by subtracting the working-fluid indicated power from the total motoring power. Overall the results remain reasonable in terms of increasing mechanical losses with increasing pressure and speed. However, the spacing between the curves is varied; this is probably due to the errors involved in the several measurements necessary to obtain the final number. Note that the results shown in figure 21 are similar in value at a given point for both helium and hydrogen. Some difference would be expected due to the higher gas work losses in the buffer space for helium as compared with hydrogen. However, this difference is small and may be lost in the measurement error.

Comparison of Mechanical Losses by Motoring and Energy-Balance Results

A comparison was made of the mechanical losses as found from energy-balance and motoring results. These are shown in figures 22 and 23 for helium and hydrogen working fluids, respectively. The energy-balance results are determined by adding the heat to the oil and the heat to the buffer-space cooling water. The curves shown are an average of those obtained for low-power baseline tests with the alternator and high-power baseline tests with the dynamometer. The motoring results are the same as those given in figure 21. They were determined by subtracting the working-fluid indicated power during motoring from the total motoring power.

For both helium and hydrogen the two methods give results that are about the same at the lower speeds, but the motoring results are significantly higher at the high speeds. Also, the energy balance gives results that vary linearly with speed, while the motoring results yield a higher-order curve.

There are deficiencies in each method. For the energy balance the heat to the buffer-space cooling water may include some conduction losses, which should not be charged against the mechanical losses. Also, the heat to the engine coolers includes some friction losses from the piston rings and displacer rod seal. These should be included in the estimate of mechanical losses but are not. The motoring tests have the problem of different loads on the bearings, piston rings, and shaft seals when compared with engine tests, as well as the problem of sorting out the gas work losses.

To minimize the differences in loading during the motoring tests, the volume of the working space was changed by removing the cooler-regenerators and by adding the volume of the holes in the displacer to give about the same pressure ratio during motoring as in engine operation. These changes are described in the Test Setup section. Figure 24 compares pressure traces for the compression and buffer spaces from motoring and engine tests. The traces are for a mean compression-space pressure of 6.9 megapascals (1000 psi), an engine speed of 3000 rpm, and helium working fluid.

The compresssion-space pressure ratio (maximum pressure/minimum pressure) was 1.99 for the engine tests and 1.95 for motoring. However, there was a difference in the phasing. The maximum pressure occurred about 17° later for

the engine tests than for motoring; the minimum pressure occurred about 31° later for the engine tests. The buffer-space pressure ratio was 1.47 for engine tests and 1.44 for motoring. The phasing was approximately the same for the buffer space. The buffer-space mean pressures are at different levels. This is a function of the pumping of the piston rings and does vary somewhat as the slots in the piston rings and the piston ring grooves become dirty, usually with a combination of oil and rust particles. The piston rings are cleaned or new rings installed when the mean buffer-space pressure becomes excessively high with respect to the mean compression-space pressure.

The pressure traces with hydrogen working fluid are the same except that the pressure ratios are slightly lower. This is shown in figure 25, which compares compression-space and buffer-space pressure traces for helium and hydrogen engine results. Again, the mean compression-space pressure is 6.9 megapascals (1000 psi), and the engine speed is 3000 rpm. The phasing is about the same for each working fluid, but the compression-space pressure ratio for hydrogen is 1.88 and that for helium is 1.99. The buffer-space pressure ratios are 1.38 for hydrogen and 1.47 for helium. The mean buffer-space pressures are again somewhat different.

The mechanical losses can be used to determine indicated power by summing the brake power and mechanical losses. Thus a further check on both methods of determining the mechanical losses is to compare the indicated power found by using the mechanical losses to that found directly from pressure-volume (p-v) diagrams. Figure 15 gives this comparison for the energy-balance results; the energy-balance results are determined by summing brake power, heat to the oil, and heat to the buffer-space cooling water. The figure shows that the indicated power by p-v diagrams is higher at high speeds and either close to or less than the energy-balance results at low speeds. This same trend is shown in figures 21 and 22, where the motoring-determined mechanical losses are greater at the high speeds than the mechanical losses determined from an energy balance and about the same or less at the low speeds.

The indicated power found from the brake power and the mechanical losses determined from the motoring results are compared in figure 26 with the indicated power found from p-v diagrams. The comparison is shown for hydrogen only. These curves are more similar in shape than were the curves compared in figure 15. However, the differential between the curves is generally greater than in figure 15. Thus the experimental data do not indicate which method of determining mechanical losses is more correct particularly when noting that some problems also remain in providing fully reliable pressure-volume diagrams for these comparisons.

With respect to measuring indicated power the three methods (p-v diagrams, summing brake power and mechanical losses from energy balances, and summing brake power and mechanical losses from motoring results) give results that are all within a reasonable experimental band but none of which can be identified as the most correct.

CONCLUDING REMARKS

The efforts to complete the full-power baseline tests were met with numerous engine and facility problems. These data are less reliable than the data taken in the low-power baseline tests and published in reference 1. It is felt that the primary reason for the differences in engine performance between these tests and the tests reported in reference 1 was poor heat exchanger performance, particularly the regenerator. However, it may be possible to obtain correlation through the use of a computer simulation if the proper adjustments

for both increased flow losses and reduced heat transfer could be made. Even without this, the low-speed data should be reasonable as the effects of degraded heat exchanger performance are less at the lower speeds.

Because of the reduced engine output the detailed test data have not been included as part of this report. However, the data are available in computer printout form from the author. A sample data point is included in the appendixes to show what is available. The changes to the information necessary to understand the data printouts are also in the appendixes. The remainder of the information needed is given in reference 1.

Motoring tests were another method investigated, in addition to using energy balances, to determine mechanical losses. Each method, motoring or energy balance, had certain deficiencies and the difference between the two was large at high speed. The indicated power found from pressure-volume diagrams was compared with that found by summing the brake power and mechanical losses. If the pressure-volume diagrams are accurate, this comparison shows that the shape of the curve based on the motoring-determined mechanical losses is more correct than the shape of the curve based on the mechanical losses from the energy balance. However, the overall differential between the curves suggests that the magnitude of the energy-balance mechanical losses is more accurate. The best estimate of the mechanical losses for this investigation may be an average of the results from the motoring and energy-balance methods.

Future test work with the GPU-3 engine will involve testing new component concepts. These include low-cost regenerators as well as a method to improve the heat transfer between the heater tubes and the combustion gases.

SUMMARY OF RESULTS

The GPU-3 Stirling engine was installed on a dynamometer test bed and tested over its full range of engine speeds and pressures at a heater-tube gas temperature of 677° C (1250° F). The mean compression-space pressure was varied from 2.8 to 6.9 megapascals (400 to 1000 psi) while engine speed was varied from 1500 to 3500 rpm. Performance figures are presented with both helium and hydrogen as the working fluid.

Motoring tests were then run after removing the cooler-regenerator cartridges and installing a special displacer piston. The purpose of these tests was to aid in determining engine mechanical losses. Tests were run with both helium and hydrogen over a range of mean compression-space pressures of 1.4 to 6.9 megapascals (200 to 1000 psi) and engine speeds of 1500 to 3500 rpm.

The major results obtained from these tests are as follows:

1. The maximum power obtained with hydrogen was 6.82 kilowatts (9.14 hp) at 6.9-megapascal (1000-psi) mean compression-space pressure and 3500-rpm engine speed. The minimum brake specific fuel consumption (bsfc) was 315 g/kW-hr (0.52 lb/hp-hr) at 6.9 megapascals (1000 psi) and 1500 rpm. This represents a brake thermal efficiency of 26.4 percent. This efficiency is in the same range as that obtained by General Motors during its testing.

2. The maximum power obtained with helium was 4.26 kilowatts (5.71 hp) at 6.9-megapascal (1000-psi) mean compression-space pressure and 2500-rpm engine speed. The minimum bsfc was 390 g/kW-hr (0.64 lb/hp-hr) at 6.9 megapascal (1000 psi) and 1500 rpm. This represents a brake thermal efficiency of 21.3 percent.

3. The engine output for these high-power baseline tests with the dynamometer was low compared with previously reported low-power baseline test results obtained with an alternator. This was primarily true at high speeds. It is felt that this was caused by degradation of heat exchanger performance due to contamination by rust and oil.

4. Engine brake thermal efficiency was higher for tests with the dynamometer than for the previous alternator testing because a noncontaminated preheater was installed to reduce combustion system losses. These lower losses more than offset the additional losses in the degraded heat exchangers of the heater head.

5. Motoring tests were run to aid in determining mechanical losses; the motoring results were compared with energy-balance estimates of the mechanical losses. The energy-balance results yielded a linear variation of mechanical losses with engine speed, but the motoring results showed a higher-order variation with speed. The mechanical losses were about the same at low speeds for each method but significantly different at high speeds. The experimental data do not indicate that one method is more correct than the other.

6. Indicated power results were obtained as a function of mean compression-space pressure and engine speed for both helium and hydrogen as the working fluid. Three methods were used: pressure-volume diagrams, summing brake power and mechanical losses from an energy balance, and summing brake power and mechanical losses from motoring results. Although it is not possible to conclude which is the most correct, all three give results that are within a reasonable experimental band.

APPENDIX A

SAMPLE DATA POINT

The detailed data taken during these tests have not been included as part of this report. However, computer printouts of the data are available from the author. A sample data point is shown here to indicate what is available.

Most of the information necessary to understand the data printouts is given in reference 1. Changes to the instrumentation for these tests are listed in table I. These are given as measurements that were removed as well as those added or changed. Figure 27 shows the new preheater thermocouple locations. In addition, the following calculations were eliminated: PWRALT, alternator output power; ALTEFF, alternator efficiency; and QCWTOC, heat out to cooling water per cycle - total flow. The calculation of PWROUT, engine output power, was changed to use the measurement of engine torque.

Finally, the explanation of the run number for each data point is the same as given in reference 1 with the following exception. The heater-tube gas temperature for each point was 1250° F, and this is identified by a "25" in the run number.

RUN NUMBER& M2S-105A DATE& */20/79 REAL TIME& 1&618

U.S. CUSTOMARY UNITS

STEADY STATE TEST DATA

RUNTIM (HR)	TAMB (F)	TGDUM2 (F)	TFINN (F)	TAINN (F)	TAINPH (F)	TOILIN (F)	TCWIN (F)
272.4	75.	1255.	82.	81.	72.	120.	66.

TDELO (F)	TOLWC (F)	TDL&B (F)	TDWFV (F)	TGBUF (F)	TGCOMP (F)	TGEXP (F)	TGDUM1 (F)	TEXHO1 (F)
4.8	13.6	7.5	4.2	164.	161.	1179.	1206.	485.

TEXHO2 (F)	TEXHO3 (F)	TPHOT1 (F)	TPHOT2 (F)	TPHOT3 (F)	TPHOB1 (F)	TPHOB2 (F)	TPHOB3 (F)
502.	435.	405.	390.	420.	288.	276.	267.

TEXHO4 (F)	TEXHO5 (F)	TEXHO6 (F)	TRH1T (F)	TRH2H (F)	TRH3B (F)	TRH4C (F)	TRH5C (F)
420.	452.	473.	1023.	0.	0.	712.	732.

TRH6C (F)	TRH7C (F)	TRH8TI (F)	TRH9HI (F)	TRH10B (F)	TCYL1T (F)	TCYL2 (F)	TCYL3 (F)	TCYL4 (F)	TCYL5B (F)
663.	728.	1024.	731.	258.	1251.	1165.	1041.	764.	566.

TCYL6C (F)	TCYL7C (F)	TCYL8C (F)	TIC1T (F)	TIC&B (F)	THT1DT (F)	THT2DH (F)	THT3DB (F)	THT4RT (F)	THT5RB (F)
1046.	1102.	&C73.	744.	522.	1419.	1417.	1467.	0.	1369.

THT6C (F)	THT7C (F)	THT8C (F)	THT9T (F)	THT10B (F)	THT11E (F)	THT12R (F)	MEANCP (PSI)	MEANBP (PSI)
1292.	1322.	1437.	1443.	1346.	1201.	1160.	1004.	993.

TORQUE (LB-FT)	RPM (RPM)	CWFLOC (GPM)	CWFLOB (GPM)	CWFLFV (GPM)	OILFLO (GPM)
19.5	1504.	3.55	.53	.62	.46

FFLO (LB/HR)	CAFLO (LB/MIN)	NAFLO (LB/HR)	POIL (PSI)	PFNOZ (PSI)	PCOAIR (IN H20)	PNOAIR (IN H20)
2.892	1.68	1.28	45.	1.3	13.0	24.6

TGDUM3 (F)
1195.

DYNAMIC TEST DATA

MINCP (PSI)	MAXCP (PSI)	MINBP (PSI)	MAXBP (PSI)	PDEXP (PSI)	AMINCP (DEG)	AMAXCP (DEG)
701.	1344.	822.	1137.	619.	293.	78.

AMINEP (DEG)	AMAXEP (DEG)	AMINBP (DEG)	AMAXBP (DEG)
295.	78.	57.	257.

STEADY STATE CALCULATIONS

OVERALL QUANTITIES

PWRIN (HP)	PWROUT (HP)	BRKEFF (%)	QCWCO (HP)
21.14	5.581	26.40	9.46

BMEP (PSI)	BSFC (LB/HP-HR)	TRATIO (DIMEN)	AFRAT (DIMEN)
201.41	.518	.379	35.3

HEAT BALANCE

QIN (FT-LB)	QRKOUT (FT-LB)	QOILC (FT-LB)	TAEXHO (F)	QEXHC (FT-LB)	QCWCOC (FT-LB)
963.80	122.96	3.95	961.2	88.05	208.08

QCWBC (FT-LB)	QCWFVC (FT-LB)	TAPREM (F)	QRADC (FT-LB)	CONVH (BTU/HR-SQ FT-F)	QCONVC (FT-LB)	QUNACC (FT-LB)
18.03	11.21	341.0	4.21	1.262	5.02	2.78

QING (BTU/HR)	QOUT (BTU/HR)	QINEM (BTU/HR)	QINEC (BTU/HR)
38029.	20932.	41231.	40824.

CONDUCTION LOSSES

QRH1 (BTU/HR)	QRH2 (BTU/HR)	QRH3 (BTU/HR)	QRH4 (BTU/HR)	QCYL1 (BTU/HR)	QCYL2 (BTU/HR)	QSHUT (BTU/HR)
.0	.0	150.8	138.3	489.5	695.5	809.8

QINSC (BTU/HR)	QDISP (BTU/HR)	QCONDT (BTU/HR)
406.6	290.1	3202.

S.I. UNITS

STEADY STATE TEST DATA

RUNTIM (HR)	TAMB (C)	TGDUM2 (C)	TFINN (C)	TAINN (C)	TAINPH (C)	TOILIN (C)	TCWIN (C)
272.9	24.	679.	38.	27.	22.	49.	20.

TDELO (C)	TDLWC (C)	TDLWB (C)	TDWFW (C)	TGBUF (C)	TGCOMP (C)	TGEXP (C)	TGDUM1 (C)	TEXH01 (C)
2.7	7.6	4.4	2.3	42.	72.	637.	652.	252.

TEXH02 (C)	TEXH03 (C)	TPH0T1 (C)	TPH0T2 (C)	TPH0T3 (C)	TPH0B1 (C)	TPH0B2 (C)	TPH0B3 (C)
261.	229.	207.	199.	216.	142.	136.	131.

TEXH04 (C)	TEXH05 (C)	TBXH06 (C)	TRH1T (C)	TRH2M (C)	TPH3B (C)	TRH4C (C)	TRH5C (C)
216.	233.	245.	551.	0.	0.	378.	389.

TRH6C (C)	TRH7C (C)	TPH8TI (C)	TRH9MI (C)	TRH10B (C)	TCYL1T (C)	TCYL2 (C)	TCYL3 (C)	TCYL4 (C)	TCYL5B (C)
351.	367.	951.	388.	126.	677.	629.	561.	407.	297.

TCYL6C (C)	TCYL7C (C)	TCYL8C (C)	TIC1T (C)	TIC2B (C)	THT1DT (C)	THT2DM (C)	THT3DB (C)	THT4RT (C)	THT5RB (C)
563.	594.	578.	396.	272.	771.	769.	797.	0.	743.

THT6C (C)	THT7C (C)	THT8C (C)	THT9T (C)	THT10B (C)	THT11E (C)	THT12R (C)	MEANCP (MPA)	MEANRP (MPA)
700.	717.	781.	784.	730.	649.	627.	6.92	6.84

TORQUE (N-M)	RPM (RPM)	GWFLOC (LPM)	GWFLOB (LPM)	GWFLFV (LPM)	OILFLO (LPM)
19.4	1504.	13.4	2.01	2.35	1.74

FFLO (G/HR)	GAFLO (G/MIN)	AAFLO (G/HR)	POIL (KPA)	PFNOZ (KPA)	PCOAIR (KPA)	PNOAIR (KPA)
1312.	702.	581.	310.	9.0	3.23	5.96

TGDUM3 (C)
696.

DYNAMIC TEST DATA

MINCP (MPA)	MAXCP (MPA)	MINBP (MPA)	MAXBP (MPA)	PDEXP (MPA)	AMINCP (DEG)	AMAXCP (DEG)
4.83	9.26	5.66	7.83	4.23	293.	79.

AMINEP (DEG)	AMAXEP (DEG)	AMINBP (DEG)	AMAXBP (DEG)
293.	73.	57.	257.

STEADY STATE CALCULATIONS

OVERALL QUANTITIES

PWRIN (KW)	PWROUT (KW)	PRMEFF (%)	QCWCO (KW)
15.76	4.162	26.40	7.07

BMEP (KPA)	BSFC (G/KW-HR)	TRATIO (DIMEN)	AFRAT (DIMEN)
1388.9	315.	.379	35.3

HEAT BALANCE

QIN (JOULES)	QRMOUT (JOULES)	QOILC (JOULES)	TAEXHO (C)	QEXHC (JOULES)	QCWCOC (JOULES)
628.45	165.93	5.35	238.	119.31	281.99

QCWBC (JOULES)	QCWFVC (JOULES)	TAPREH (C)	QRADC (JOULES)	CONVH (WATTS/SQ M-C)	QCONVC (JOULES)	QUNACC (JOULES)
29.43	15.20	172.	5.71	2.2180	6.80	3.77

QING (WATTS)	QOUT (WATTS)	QINEH (WATTS)	QINEC (WATTS)
11139.	6131.	12077.	11958.

CONDUCTION LOSSES

QRH1 (WATTS)	QRH2 (WATTS)	QRH3 (WATTS)	QRH4 (WATTS)	QCYL1 (WATTS)	QCYL2 (WATTS)	QSHUT (WATTS)
.0	.0	44.2	40.5	183.4	203.7	237.2

QINSC (WATTS)	QDISP (WATTS)	QCONDT (WATTS)
119.1	85.0	938.

APPENDIX B

WORKING FLUID SAMPLES

At various times during the engine tests, working-fluid samples were taken before and after engine runs. The sample bottle was evacuated, and the sample was then taken from the engine vent line. The samples were analyzed with a mass spectrometer. Typical samples for helium and hydrogen working fluids are given below.

For helium working fluid the test conditions were

Heater-tube gas temperature, °C (°F) 677 (1250)
Mean compression-space pressure, MPa (psi) 2.8 (400)
Engine s eed, rpm 2000

These conditions were held for about 2 hours before the final sample was taken.

	Before run	After run
	Working-fluid content, ppm	
H_2	0	0
He	Parent	Parent
CH_4	0	0
N_2	901	968
O_2	0	130
Ar	0	24
CO_2	29	99

For hydrogen working fluid the test conditions were

Heater-tube gas temperature, °C (°F) 677 (1250)
Mean compression-space pressure, MPa (psi) 5.5 (800)
Engine speed, rpm . . . . . 1500 to 3500

These samples were taken before and after obtaining the 5.5-megapascal (800-psi) hydrogen test data shown in this report. The total engine run time for this test was 2 hours and 50 minutes.

	Before run	After run
	Working-fluid content, ppm	
H_2	Parent	Parent
He	0	884
CH_4	94	426
N_2	5503	6179
O_2	51	50
Ar	0	95
CO_2	0	0

REFERENCES

1. Thieme, Lanny G.: Low-Power Baseline Test Results for the GPU-3 Stirling Engine. NASA TM-79103, DOE/NASA/1040-79/6, 1979.

2. Cairelli, J. E.; Thieme, L. G.; and Walter, R. J.: Initial Test Results with a Single-Cylinder Rhombic-Drive Stirling Engine. NASA TM-78919, DOE/NASA/1040-78/1, 1978.

3. Tew, Roy; Jeffries, Kent; and Miao, David: A Stirling Engine Computer Model for Performance Calculations. NASA TM-78884, DOE/NASA/1011-78/24, 1978.

4. Tew, Roy C., Jr.; Thieme, Lanny G.; and Miao, David: Initial Comparison of Single-Cylinder Stirling Engine Computer Model Predictions with Test Results. NASA TM-79044, DOE/NASA/1040-78/30, 1979.

5. Rice, William J.: Indicated Mean-Effective Pressure Instrument. NASA Tech Brief B76-10542, 1977.

6. Rice, William J; and Birchenough, Arthur G.: Modular Instrumentation System for Real-Time Measurements and Control on Reciprocating Engines. NASA TP-1757, 1980.

7. Percival, W. H.: Historical Review of Stirling Engine Development in the United States from 1960 to 1970. (REPT-4-E8-00595, General Motors Research Labs.; EPA Contract EPA-4-E8-00595.) NASA CR-121097, 1974.

TABLE I. - CHANGES TO GPU-3 INSTRUMENTATION FOR DYNAMOMETER TESTS

[All thermocouples are Chromel-Alumel (type K). Listed ranges are full-scale range for pressure transducers and load cell and measurement range for thermocouples. Maximum pressures (items 94 and 95) are found by adding the pressure swing determined by the miniature transducers to the values of minimum pressure (items 92 and 93).]

(a) Removed

Mnemonic	Parameters
TALTH	Alternator housing temperature
TDLWT	Cooling-water delta temperature - total flow out to in
	Preheater inside surface temperature:
TPHIT1	Top - 0°
TPHIT2	Top - 120°
TPHIT3	Top - 240°
TPHIB1	Bottom - 0°
TPHIB2	Bottom - 120°
TPHIB3	Bottom - 240°
AMP	Alternator output current
VOLT	Alternator output voltage
CWFLOT	Cooling-water flow - total
RLOAD	Resistance load bank setting
PDCOMP	Pressure swing (minimum to maximum) - compression space
PDBUF	Pressure swing - buffer space

(b) Added or changed

Item	Mnemonic	Parameter	Instrument	Range
		Exhaust temperature out of preheater:	Thermocouple	350°-600° F
85	TEXH01	0°	↓	↓
86	TEXH02	60°		
87	TEXH03	120°		
88	TEXH04	180°		
89	TEXH05	240°		
90	TEXH06	300°		
91	TORQUE	Engine torque	Load cell	0-50 lb (0-75 lb-ft)
92	MINCP	Minimum compression-space pressure	Strain-gage transducer	0-1000 psig
93	MINBP	Minimum buffer-space pressure	Strain-gage transducer	0-1000 psig
94	MAXCP	Maximum compression-space pressure	Miniature strain-gage transducer	0-2000 psig
95	MAXBP	Maximum buffer-space pressure	Miniature strain-gage transducer	0-2000 psig

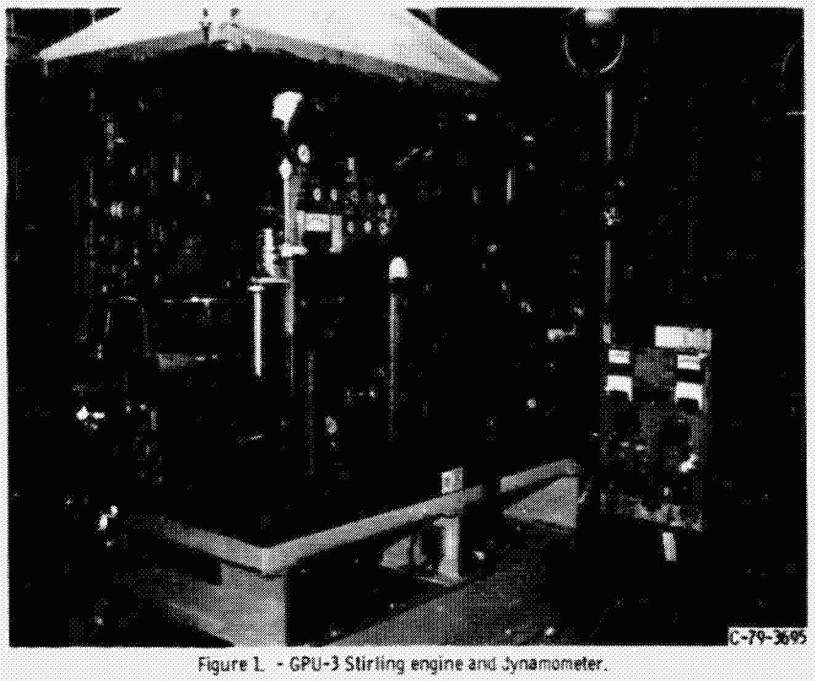

Figure 1. - GPU-3 Stirling engine and dynamometer.

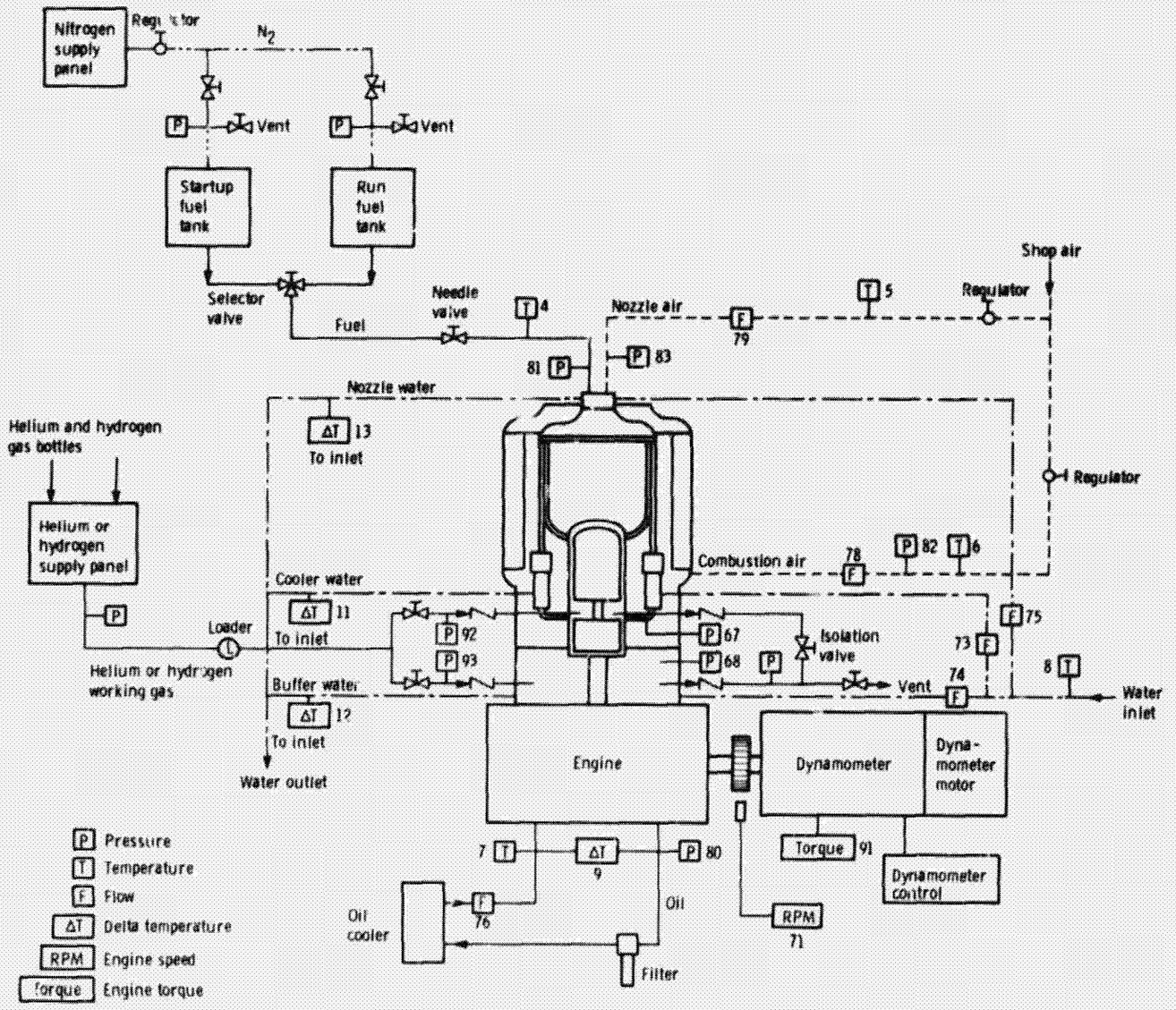

Figure 2. - GPU-3 test schematic.

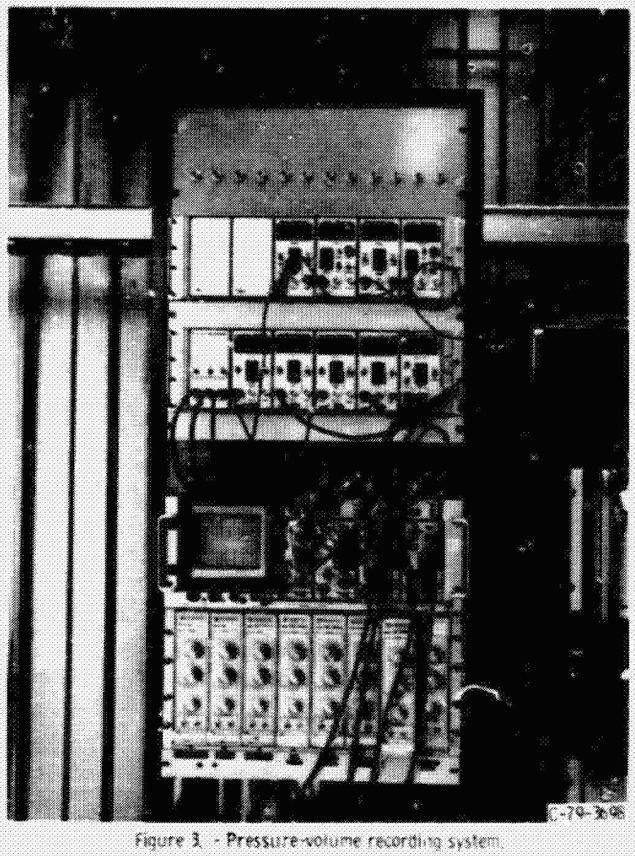

Figure 3. - Pressure-volume recording system.

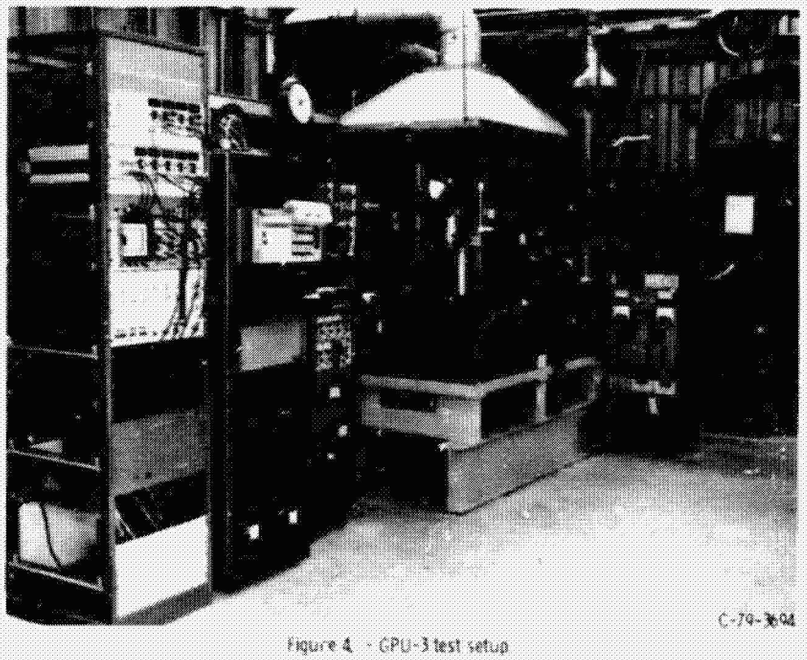

Figure 4. - GPU-3 test setup.

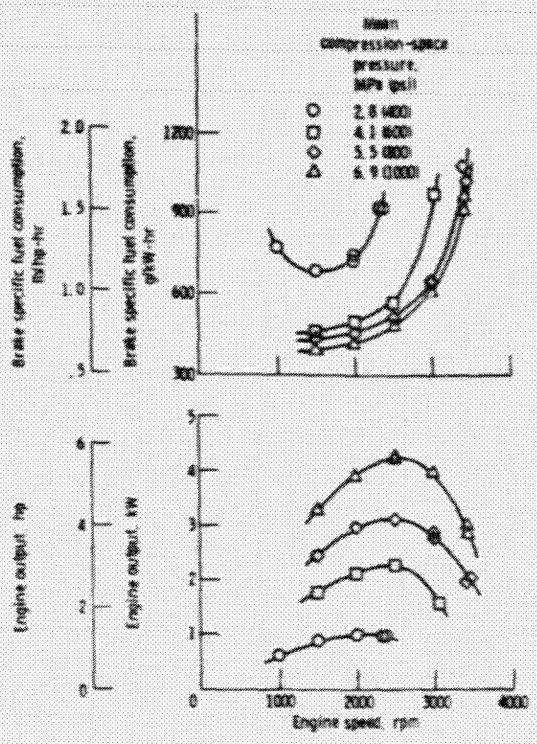

Figure 5. - Helium engine performance as a function of engine speed and mean compression-space pressure for a heater-tube gas temperature of 677° C (1250° F) and a water inlet temperature of 20° C (68° F).

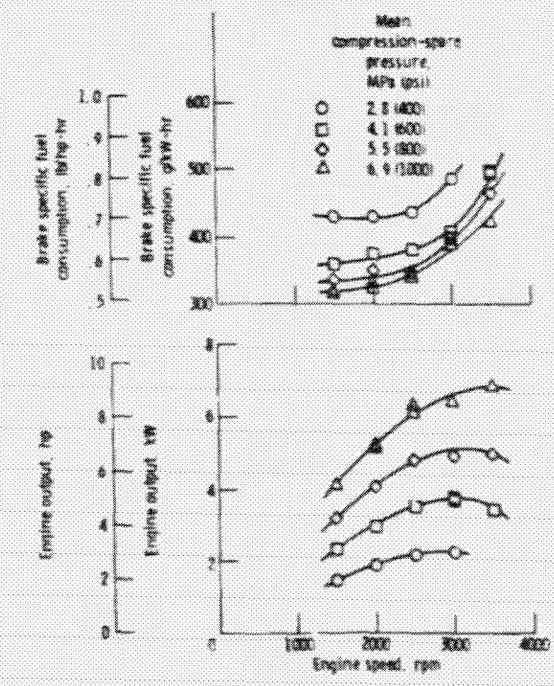

Figure 6. - Hydrogen engine performance as a function of engine speed and mean compression-space pressure for a heater-tube gas temperature of 677° C (1250° F) and a water inlet temperature of 20° C (68° F).

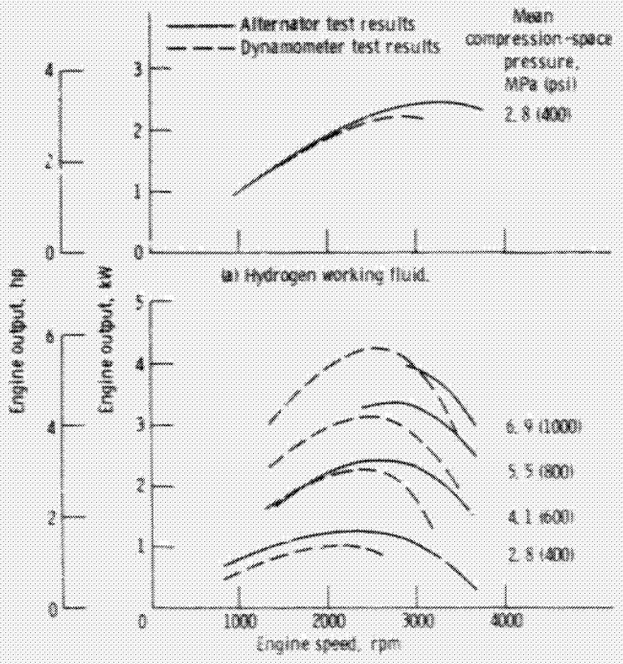

(a) Hydrogen working fluid.

(b) Helium working fluid.

Figure 7. - Comparison of engine output with previous low-power alternator test results for both helium and hydrogen working fluids. Alternator test conditions: heater-tube gas temperature, 650° C (1200° F); water inlet temperature, 13°-15° C (56°-59° F). Dynamometer test conditions: heater-tube gas temperature, 677° C (1250° F); water inlet temperature, 20° C (68° F).

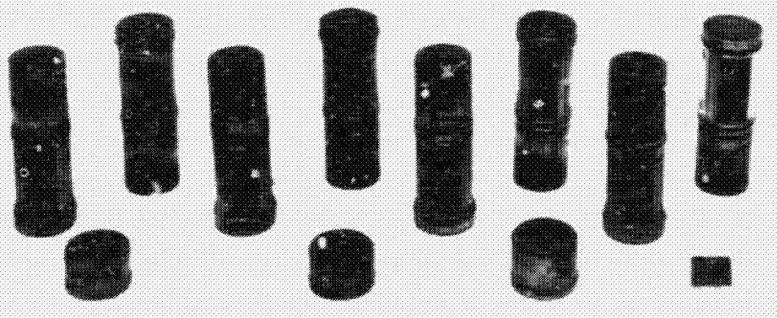

C-80-1442

Figure 8. - GPU-3 cooler-regenerator cartridges after 191 hours of testing.

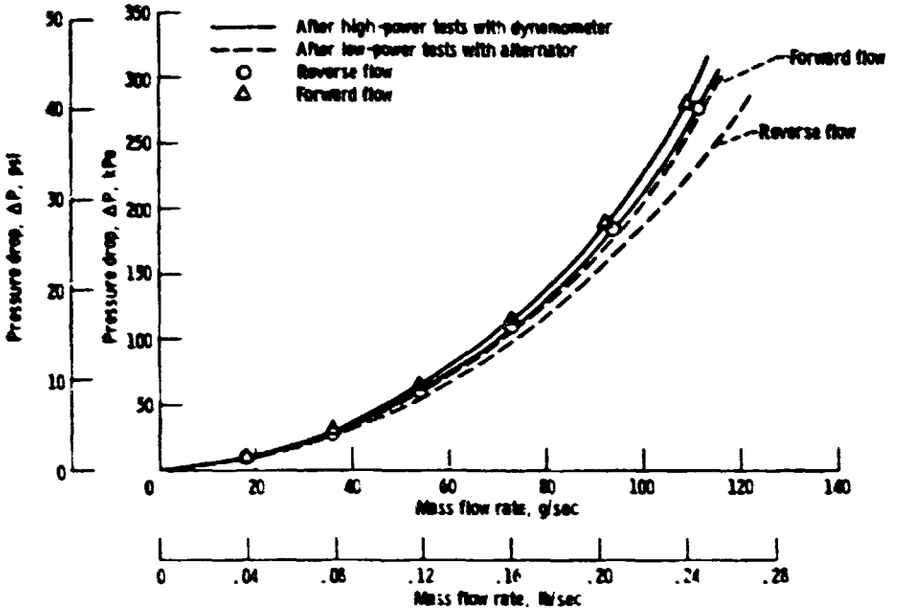

Figure 9. - Comparison of pressure drop as a function of mass flow rate for the heater head assembly after low-power tests with alternator and after high-power tests with dynamometer. Air at 115-psi inlet; forward flow from compression space to expansion space.

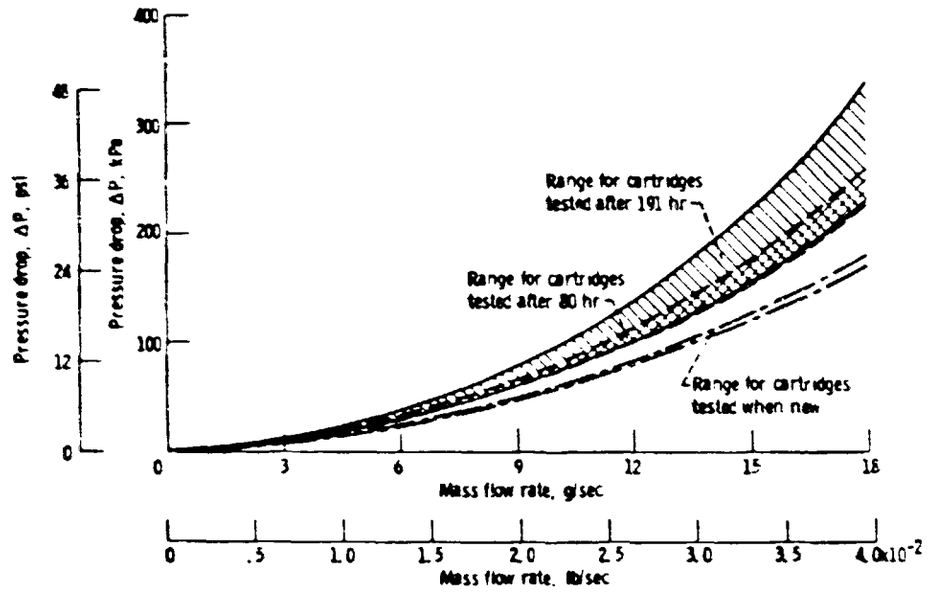

Figure 10. - Pressure drop as a function of mass flow rate for three cooler-regenerator cartridges when new, after 80 hours of testing, and after 191 hours of testing. Air at 115-psi inlet; data for forward flow only (from cooler to regenerator).

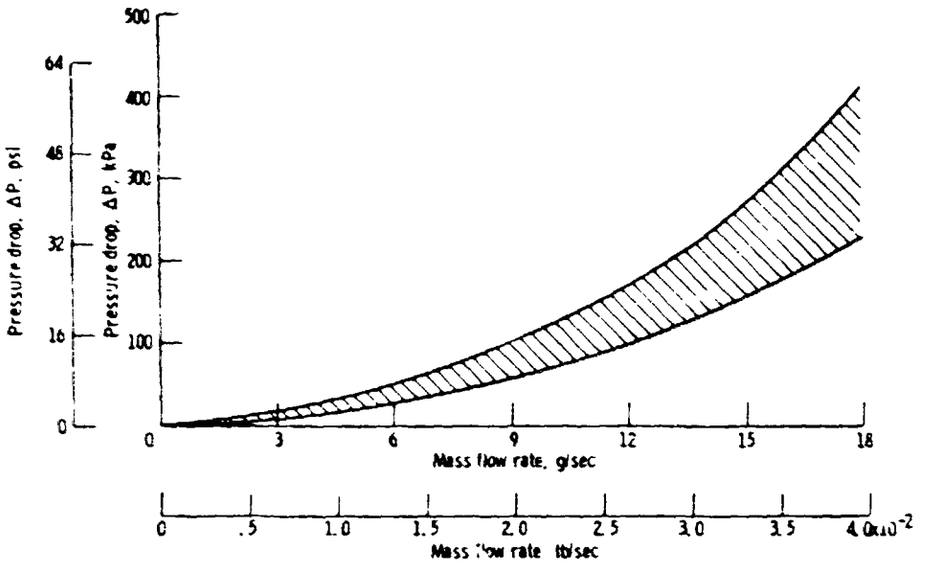

Figure 11 - Range of pressure drop as a function of mass flow rate for eight cooler-regenerator cartridges after 191 hours of testing. Air at 115-psi inlet; data for reverse flow only (from regenerator to cooler).

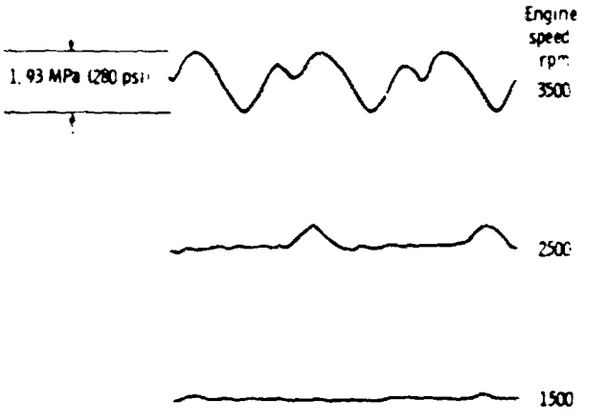

Figure 12 - Pressure oscillations in common vent line for buffer and compression spaces. Working fluid, hydrogen, mean compression-space pressure, 5.5 MPa (800 psi). (Recording speed was different for each trace; also, starting point does not correspond for each trace; amplitude scale is the same.)

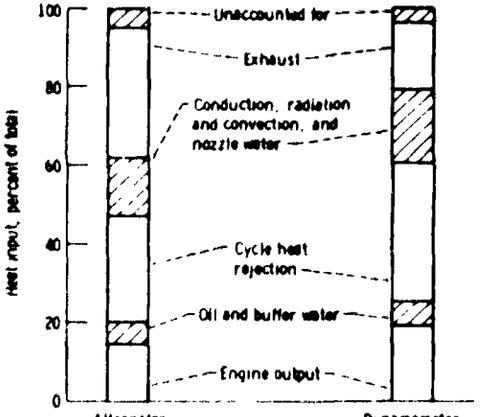

Engine output, kW (hp)	1.47 (1.97)	1.44 (1.93)
Heater-tube gas temperature, °C (°F)	650 (1200)	677 (1250)
Cooling-water inlet temperature, °C (°F)	15 (59)	20 (68)

Figure 13. - Comparison of energy balances for alternator and dynamometer test results. Working fluid, hydrogen; mean compression-space pressure, 2.8 MPa (400 psi); engine speed, 1500 rpm.

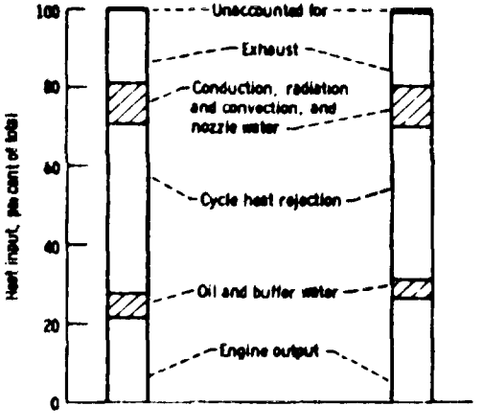

Engine output, kW (hp): 3.29 (4.42) 4.16 (5.58)

Figure 14. - Energy balances for helium and hydrogen working fluids at the maximum efficiency point for each. Heater-tube gas temperature, 677 °C (1250 °F); cooling-water inlet temperature, 20 °C (68 °F); mean compression-space pressure, 6.9 MPa (1000 psi); engine speed, 1500 rpm.

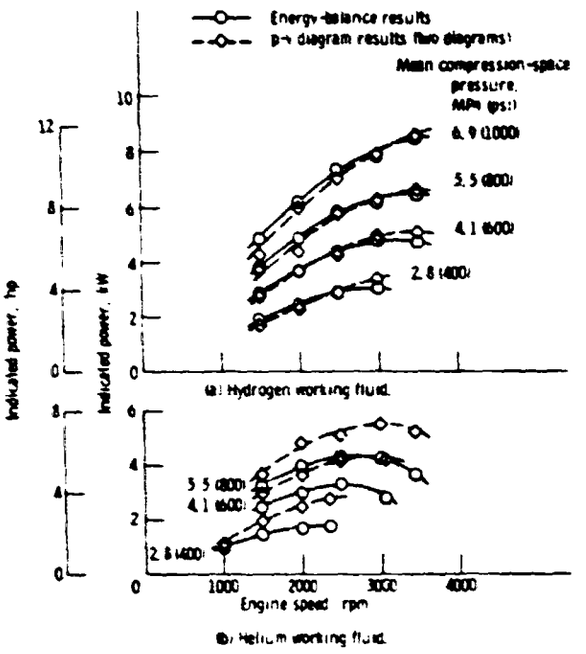

Figure 15. - Indicated power as a function of engine speed and mean compression-space pressure for helium and hydrogen working fluids. Comparison of energy-balance results with pressure-volume diagram results.

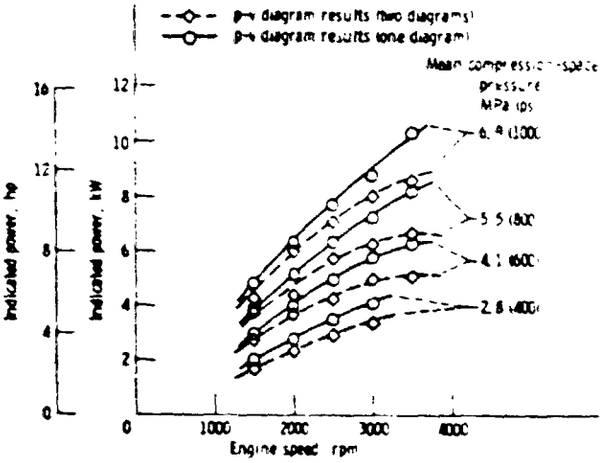

Figure 16. - Comparison of indicated power results from pressure-volume diagrams using one and two diagrams for hydrogen working fluid.

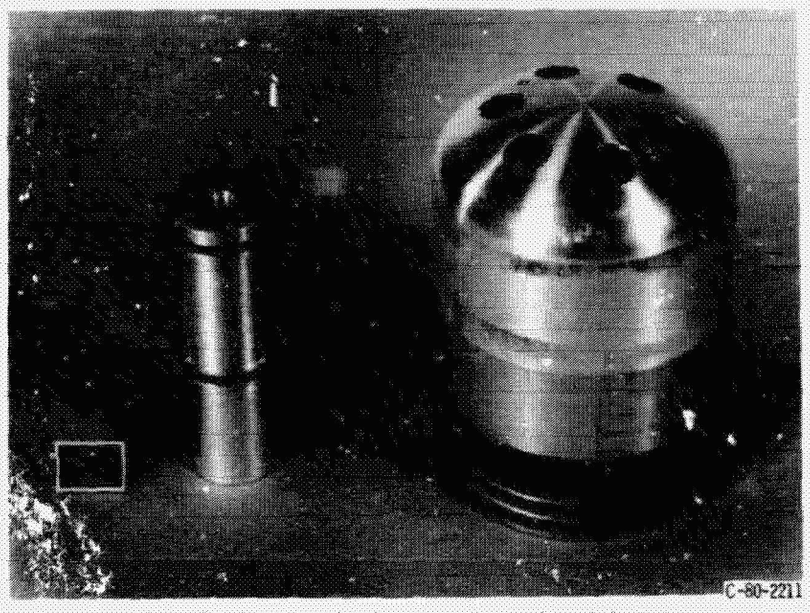

Figure 17. - Displacer and cooler-regenerator plug for motoring tests.

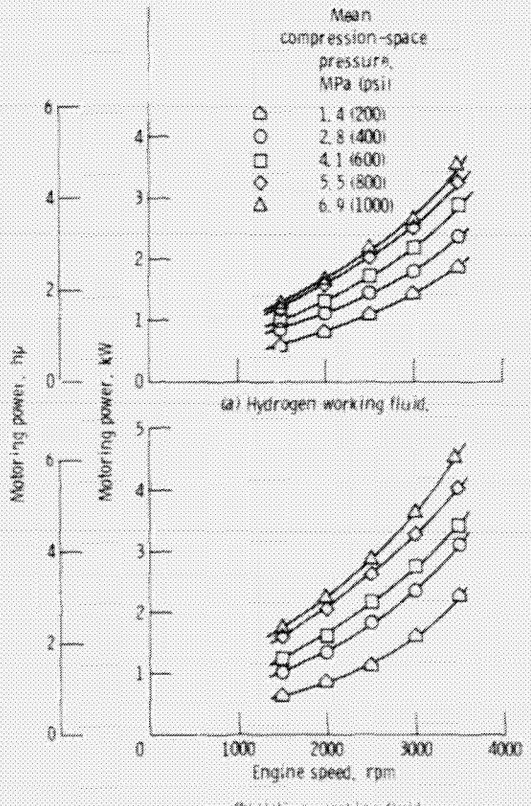

(a) Hydrogen working fluid.

(b) Helium working fluid.

Figure 18. - Motoring power as a function of mean compression-space pressure and engine speed for both helium and hydrogen working fluids.

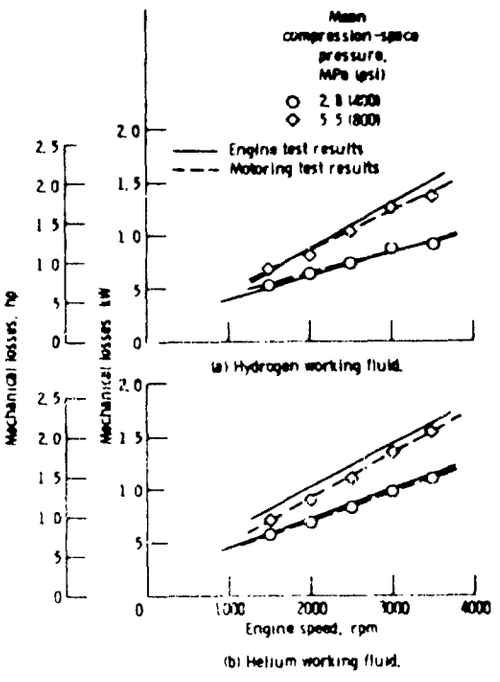

Figure 19. Comparison of mechanical losses as determined by energy balances (heat to oil + heat to buffer water) for motoring tests and engine tests.

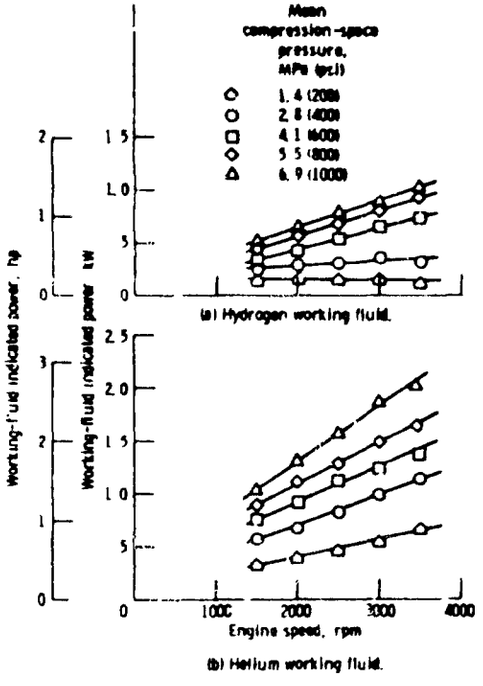

Figure 20. - Working-fluid indicated power for motoring tests as a function of mean compression-space pressure and engine speed for both helium and hydrogen working fluids.

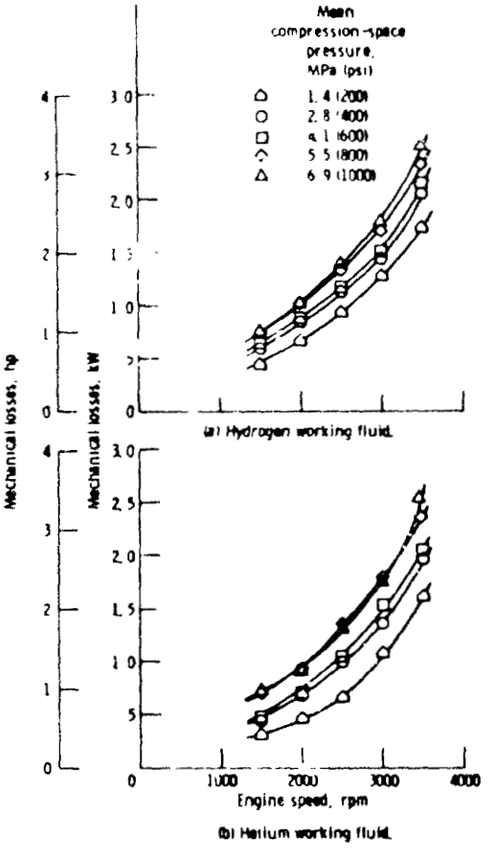

Figure 21 - Mechanical losses as determined by the difference in motoring power and working-fluid indicated power as a function of mean compression-space pressure and engine speed for both helium and hydrogen working fluids.

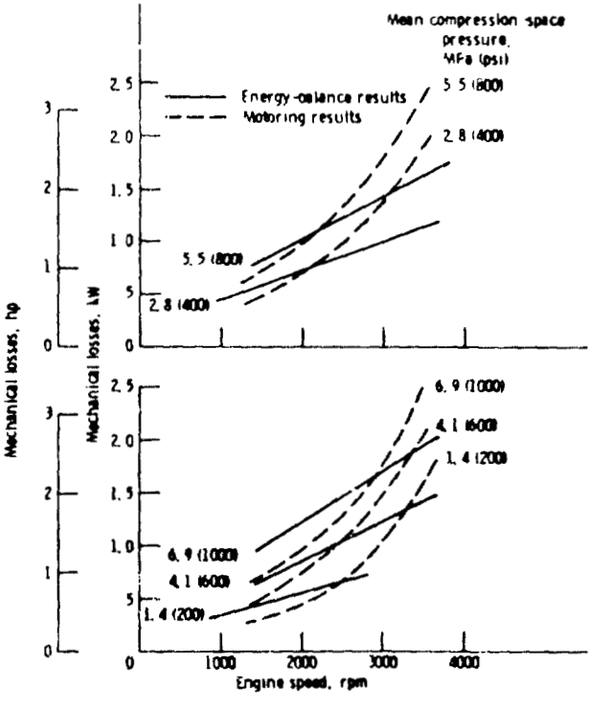

Figure 22. - Comparison of mechanical losses as determined by energy-balance and motoring results for helium working fluid.

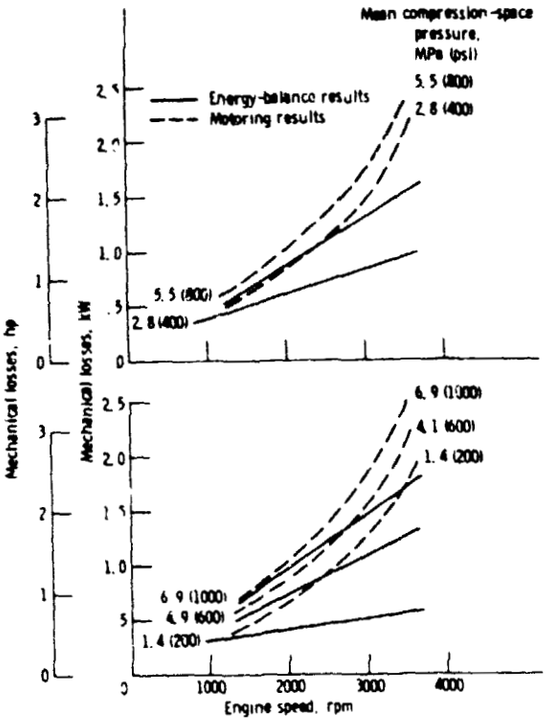

Figure 23. - Comparison of mechanical losses as determined by energy-balance and motoring results for hydrogen working fluid.

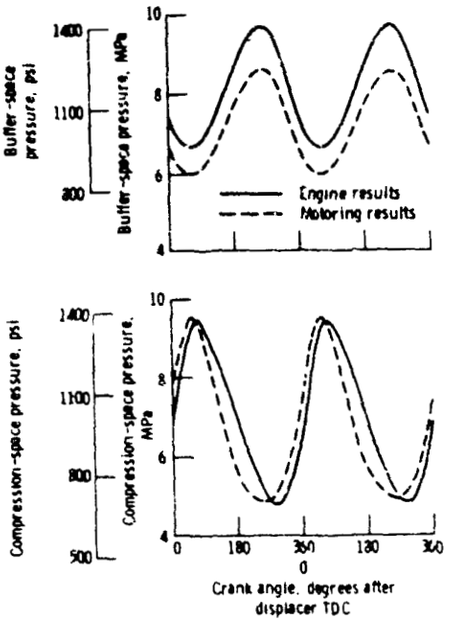

Figure 24. - Comparison of compression-space and buffer-space pressure traces for engine and motoring tests. Working fluid, helium; mean compression-space pressure, 6.9 MPa (1000 psi); engine speed, 3000 rpm.

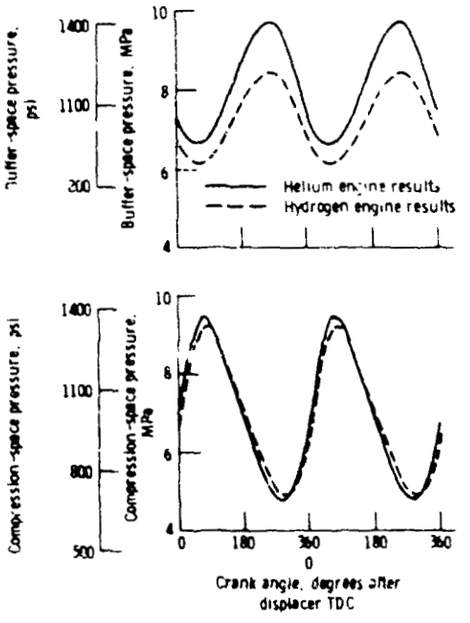

Figure 25. - Comparison of compression-space and buffer-space pressure traces for engine tests with helium and hydrogen working fluids. Mean compression-space pressure, 6.9 MPa (1000 psi); engine speed, 3000 rpm.

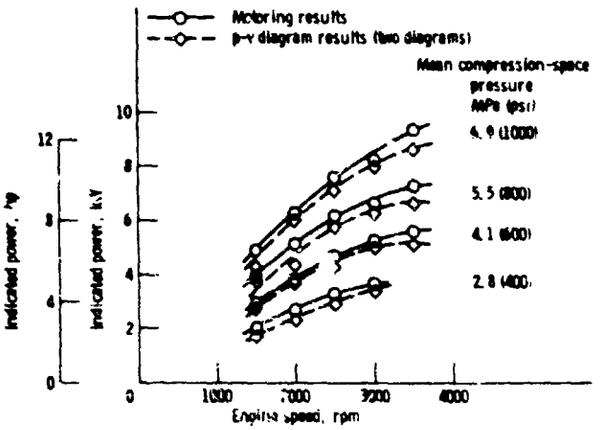

Figure 26. - Comparison of indicated power from pressure-volume diagrams and by using motoring results for hydrogen working fluid.

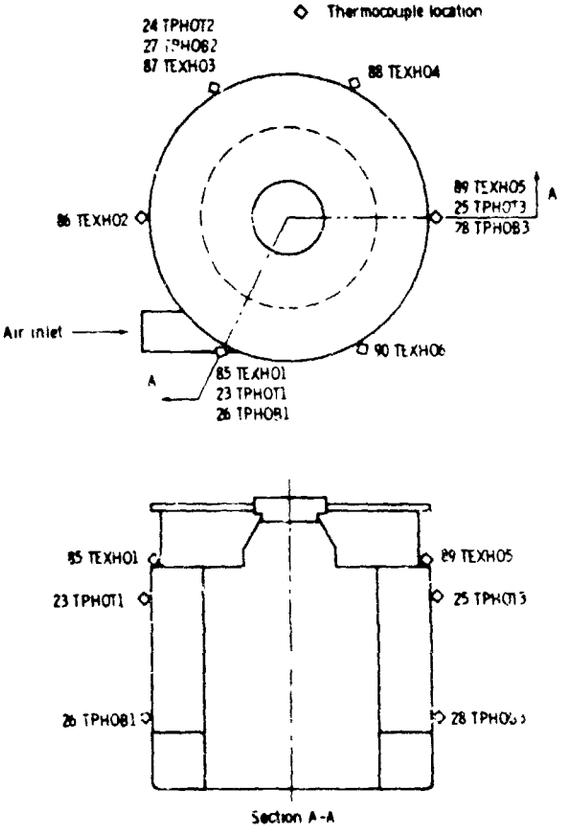

Figure 27 - GPU-3 preheater thermocouple locations